

Mott transition and superexchange mechanism in magnetically doped $X\text{Si}_2\text{N}_4$ caused by large $3d$ orbital onsite Coulomb interaction

Yijun Wang,¹ Dominik Legut², Xiaopeng Liu¹, Yiyao Li,¹ Chenxi Li,¹ Yiliu Sun,¹
Ruifeng Zhang¹, and Qianfan Zhang^{1,*}

¹*School of Materials Science and Engineering, Beihang University, Beijing 100191, People's Republic of China*
²*IT4Innovations, VSB-Technical University of Ostrava, 17.listopadu 2172/15, CZ-70800 Ostrava-Poruba, Czech Republic*

 (Received 11 April 2022; revised 21 July 2022; accepted 31 August 2022; published 19 September 2022)

Magnetic two-dimensional materials have great potential in the preparation of nanoelectronic and spintronic devices. Recently, a new two-dimensional material with no corresponding bulk-structure, MoSi_2N_4 , has been prepared, attracting public attention to the $X\text{A}_2\text{Z}_4$ series of materials. Naturally, doping with $3d$ magnetic element will result in various magnetic orderings. In our work, we replaced the Mo element with different transition-metal elements whose property varies from magnetic to nonmagnetic and screened out a variety of two-dimensional exchange scenarios. Then, we provided an analysis that shows the existence of a huge on-site Coulomb interaction at $3d$ orbitals which is strongly related to the Mott transition and therefore causes the superexchange interaction.

DOI: [10.1103/PhysRevB.106.104421](https://doi.org/10.1103/PhysRevB.106.104421)

I. INTRODUCTION

Materials having two-dimensional layered structures, such as graphene [1], boron nitride [2], and transition-metal chalcogenides [3], have recently attracted a great deal of attention due to their outstanding electrical and optical properties. They have a wide range of applications in multiple prospects of high-tech industries like electronics and aerospace. Correspondingly, various kinds of two-dimensional materials, such as CrI_3 [4] and transition-metal dichalcogenides [5], exhibit many novel magnetic properties rarely found in three-dimensional materials.

Recently, a new two-dimensional material with no corresponding bulk structure- MoSi_2N_4 [6] has been prepared. Following that, a series of the two-dimensional van der Waals layered materials with the same crystal structure as MoSi_2N_4 - $X\text{A}_2\text{Z}_4$ have been investigated. A number of interesting properties were found in this series of materials, e.g., the spin-valley coupling effect [7] and piezoelectric characteristics [8]. Accordingly, people have discovered novel magnetic properties in this class of materials, and realized tunable electronic and magnetic properties via many different ways, such as atomic adsorption, vacancies constructing, etc. [9–11] The discovery of two-dimensional Mott insulators [12] as well as strong correlations between magnetism and the Mott mechanism, are also compelling topics these days, such as demonstrated in CoO [13].

In two-dimensional magnetic materials, the Coulomb energy of the $3d$ orbitals, which is usually described within the Hubbard U model, its value, is one of the most crucial parameters in many other phenomena inside materials, such as the Mott transition and the superexchange mechanism. The Mott transition is primarily induced by the band splitting depending

on the U value, and the occupancy of the band states is closely related to it. The lack of relevant research results in our insufficient understanding of the semiconductor mechanism's formation process inside the materials, which restricts us to further discover more magnetic semiconductor materials with better performance. On the other aspect, the superexchange interaction is the key mechanism that determines the magnetic properties, which has been explored since the applicability of the Goodenough-Kanamori-Anderson (GKA) rule [14]. Another less-studied aspect is the role of ligands in regulating magnetic properties, which is essential to understand and control exchange coupling, especially in low-dimensional systems. This also limits the applicability of the two-dimensional magnetic materials, as the Curie temperature is often very low and there are difficulties in forming a stable long-range magnetic order.

In this work, we replaced Mo with different metal elements X to form $X\text{Si}_2\text{N}_4$ materials, in which X refers to Ti, V, Cr, Mn, Fe, Co, Ni, and Cu, explored their respective magnetic properties, and finally screened out a variety of excellent and stable properties in two-dimensional magnetic materials. Further, in the calculation process in combination with the Wannier function, we discovered that the band-structure formation mechanism inside the material is the Mott mechanism. Finally, through the investigation of material properties under various conditions and analysis of the superexchange mechanism, we explained the result of the internal magnetic order inside the material, then gained a deeper understanding of the internal magnetic order's formation process.

II. CALCULATING METHOD

The first-principles calculation has been performed in the framework of density-functional theory (DFT) using the Vienna *Ab initio* Simulation Package (VASP) [15,16]. For the electron-electron correlation effects we used the

*Corresponding author: qianfan@buaa.edu.cn

generalized gradient approximation exchange correlation as parametrized by the Perdew-Burke-Ernzerhof [17]. The projector augmented-wave pseudopotentials method [18,19] was adopted to describe the interaction between electrons and nuclei. The criteria of the total energy convergence and the atomic force tolerance were set to 10^{-4} eV and 0.01 eV/Å, respectively, and the energy cutoff of 500 eV was set on the plane-wave basis. In the process of the geometry relaxation of all structures, the $18 \times 18 \times 1$ Γ -centered Monkhorst-Pack grids [20] were employed to sample the Brillouin zone. The DFT+ U method [21] was adopted to describe the localized nature of $3d$ electrons for transition metals. The effective U - J value was set depending on the result of the linear-response method [22] and is further obtained based on the method raised by Marzari to make the value self-consistent [23]. The phonon spectra were additionally simulated employing the PHONOPY [24] code based on the finite displacement method within $4 \times 4 \times 1$ supercell, in order to verify their dynamical stability. In the calculation process, the VASP code was used to help analyze and integrate the data of density of states and the band structure [25]. We used the similar simulation scheme to calculate the energy of different phases in MoS_2 and $\text{MXene}(\text{Ti}_2\text{CO}_2)$ to make sure that our calculations are accurate, and the results are shown as Fig. S1 [26].

III. SEARCH OF STABLE STRUCTURE AND THE QUANTITATIVE STUDY OF MAGNETIC ORDERING

We first identified the stable geometries of $X\text{Si}_2\text{N}_4$ monolayer materials ($X = \text{Ti}, \text{V}, \text{Cr}, \text{Mn}, \text{Fe}, \text{Co}, \text{Ni}, \text{Cu}$), which are made up of seven layers of atoms. We chose these transition-metal atoms X because they have similar binding mode with Mo atom, and hence the $X\text{Si}_2\text{N}_4$ series materials we studied should have a similar composition pattern with that of MoSi_2N_4 . In the $X\text{Si}_2\text{N}_4$ class of materials, it has already been found that the three central atomic layers in this class of materials N-X-N share the similar patterns with that of the layered MoS_2 [27]. Therefore, based on the two stable phases of MoS_2 , we divided the different phases of materials into two categories, i.e., H and T ones. Then, combining with the different composition patterns of the leftover Si and N atoms, there are six potential structures, as shown in Fig. 1(a), named H1, H2, H3, T1, T2, and T3.

Then, we performed structural optimization by considering all six monolayer candidates for each composition constructed above. We set up the energy of H1 as the reference energy, and then the ΔE describes the energy where $\Delta E = E_{\text{st}} - E_{\text{H1}}$, in which st = H2, H3, T1, T2, or T3. In Fig. 1(b), we show that $X\text{Si}_2\text{N}_4$ tends to form the H1-type structure for $X = \text{Mo}, \text{Cr},$ and V . For all the other X elements we investigated, the T1-type structures are energetically preferred. Then, after arranging the elements X by their atomic number Z , some rules about the energy of the phases in different materials can be found. It can be clearly seen that the stable H1 structure only exists in the elements whose valence electrons are composed of three or four d electrons. For elements with 2–4 $3d$ electrons, it can be seen that ΔE for structures T1–T3 raises gradually with the increase of $3d$ electrons, from a negative value to a positive one. This is in contrast in tendency for elements with 4–8 electrons.

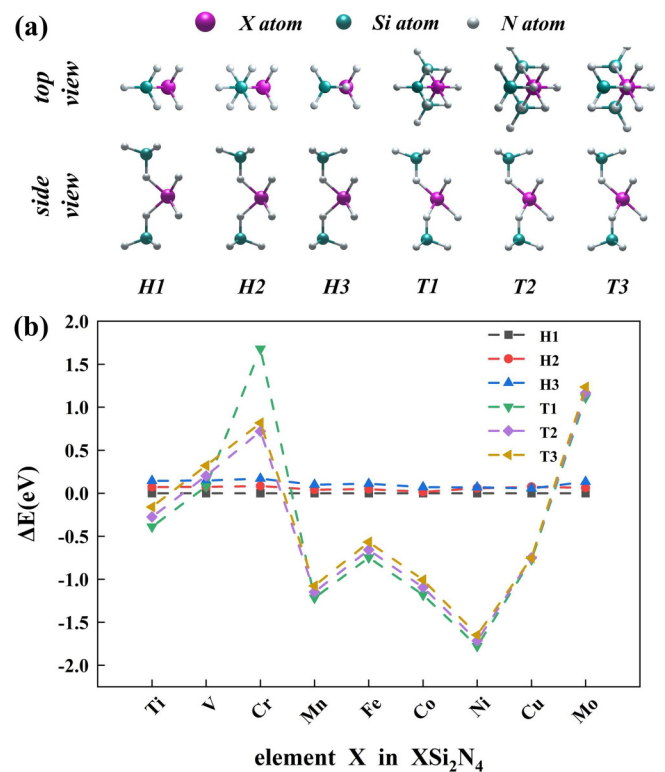


FIG. 1. (a) Possible structures of $X\text{Si}_2\text{N}_4$ series materials, and (b) the energy difference of all structures with respect to the H1 structure.

Next, we calculated the magnitude of magnetic moments of different materials on various structures, which are summarized in Table I. For $X = \text{Ti}$ or Mo , the magnetic moments for all phases are 0, indicating their nonmagnetic nature. In contrast for $X = \text{Cr}$ or Ni , the material possesses a large magnetic moment in T1–T3 and H1–H3 structures, respectively. All $X = \text{Fe}$ or Mn phases exhibit ferromagnetic ordering with relatively large magnetic moments as anticipated. For compounds with $X = \text{V}, \text{Cu},$ and Co , we identify small magnetic moments of approximately $1.0 \mu_B/\text{atom}$. It is worth noting that FeSi_2N_4 and MnSi_2N_4 have the highest magnetic moments, and VSi_2N_4 is a typical material which is one with a few d electrons and becoming spin polarized for H1–H3

TABLE I. Metal atom's magnetic moments of different materials in different phase structures (unit: μ_B/atom).

	H1	H2	H3	T1	T2	T3
TiSi_2N_4	0.0	0.0	0.0	0.0	0.0	0.0
VSi_2N_4	1.0	1.0	1.0	0.0	0.1	0.2
CrSi_2N_4	0.0	0.0	0.0	1.6	1.6	1.7
MnSi_2N_4	3.0	2.7	2.7	3.0	3.0	3.0
FeSi_2N_4	1.4	1.4	1.4	2.0	2.0	2.0
CoSi_2N_4	0.0	0.0	0.0	1.0	1.0	1.0
NiSi_2N_4	1.2	1.0	0.9	0.0	0.0	0.0
CuSi_2N_4	0.3	0.8	1.0	1.0	0.9	0.7
MoSi_2N_4	0.0	0.0	0.0	0.0	0.0	0.0

structures. Therefore, we decided to put our attention on $X = \text{Fe}$, Mn , and V for their great potential in novel and excellent magnetic properties and do further research in these kinds of materials.

The metal elements that we studied are all transition metals, whose $3d$ orbitals are partially filled with electrons. However, the traditional DFT calculation method often fails to take into account the strong Coulomb repulsion between d electrons or f electrons. Therefore, a Hubbard model [local-density approximation (LDA+ U) method] for electron-electron interactions of $3d$ electrons is required.

Firstly, we explicitly focused on the on-site Coulomb interaction in Mott insulators, which is responsible for the unauthentic gap within LDA. The energy of LDA+ U approach can be achieved by

$$E_{\text{LDA}+U}[n(r)] = E_{\text{LDA}}[n(r)] + E_{\text{hub}}[n_m^{X\sigma}] - E_{\text{DC}}[\{n^{X\sigma}\}], \quad (1)$$

in which $n(r)$ is the electronic density and $n_m^{X\sigma}$ is the atomic orbital occupations for the atom X experiencing the ‘‘Hubbard’’ term. And, in the response-function language, the value of U can be described as

$$U = \frac{\partial \alpha^{KS}}{\partial q} - \frac{\partial \alpha}{\partial q} = \chi_0^{-1} - \chi^{-1}, \quad (2)$$

in which χ_0 means the slope of the interacting response state, and χ means that of the bare response state. As a consequence, we may use the linear-response approach to get the U value.

However, there exist some problems in the process, which is whether the U value we obtain from the formula above can reflect the occupancy energy of the material. This is related for the case where α is small enough, which is indeed hard to achieve in the calculation process. Therefore, we utilized the following formula below to make the U value self-consistent:

$$U_{\text{out}} = \frac{d^2 E_{\text{quad}}}{d(\lambda_T^I)^2} = U_{\text{scf}} - \frac{U_{\text{in}}}{m}, \quad (3)$$

in which λ represents the energy with respect to on-site occupations, and m represents the effective degeneracy of the orbitals whose population changes during the process of perturbation. Then, it can be clearly seen that there is a linear correlation between U_{in} and U_{out} . The U_{scf} is the intercept of the $U_{\text{in}}-U_{\text{out}}$ curve in the meantime, which is the result we want to get.

Using this method, we measured the U value of the material for $X = \text{Fe}$, Mn , and V . The results are shown in Fig. 2. For FeSi_2N_4 , the U value obtained through linear fitting and extrapolation of data points is 7.08 eV. For MnSi_2N_4 and VSi_2N_4 , the U values are 5.01 and 5.28 eV, respectively. This gives us a roadmap for simulating the characteristics of the three materials more precisely. Meanwhile, it is worth noting that the U values amount to a relatively large value, especially for FeSi_2N_4 , which is slightly beyond a general range for materials with $3d$ electrons. The simulation results indicate that these three materials have strong nonmetallic properties and enjoy a broader application prospect in semiconductors, thermal insulation materials, and so on.

Then, we calculated the phonon spectra under the linear-response value of U and the spin-polarized state, and the

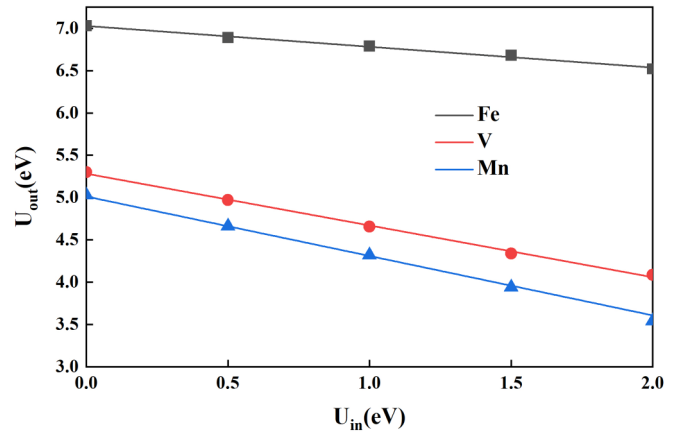


FIG. 2. Linear response of FeSi_2N_4 , MnSi_2N_4 , and VSi_2N_4 .

results are shown in Fig. S2 [26]. All these phonon spectra reveal that there is no imaginary frequency, indicating that these three materials are all dynamically stable. Furthermore, due to the small energy difference between the structure H1 and T1 of VSi_2N_4 , the possibility of phase-changing phenomenon does exist. Then, we have studied the phonon spectrum of the T1 structure of VSi_2N_4 and found that it is also stable, indicating that the phase changing in VSi_2N_4 is possible to occur. In the meantime, we observed that in VSi_2N_4 , the most stable phase changes from H1 to T1 under the linear-response U value of 5.28 eV. However, we still use the H1 phase to do further investigation. Firstly, there is only a small energy difference between the two phases of VSi_2N_4 and both of them exhibit dynamical stability according to the phonon spectrum simulation result. Secondly, the magnetic moment for the T1 phase of VSi_2N_4 is 0, which means that it does not have considerable potential for the application on two-dimensional magnetic materials.

Next, we simulated projected density of states (PDOS) to analyze the electron arrangement of the three materials, and revealed the formation process of the magnetic moment, which is shown in Fig. 3(a) and Figs. S3(a)–S3(c) [26]. From the analysis of the material structure, it can be seen that the central metal atom can provide four outermost electrons to bind with the neighboring N atoms, that is, the four electrons of $4s^2 3d^2$ are given. To prove that, it can be clearly seen that the $d-p$ hybrid orbital exists in all three materials. The hybrid effects of the $d_{xy}/d_{x^2-y^2}$ and d_{xz}/d_{yz} in $3d$ orbitals of the metal atom and p_x/p_y orbitals in $2p$ orbitals of the N atom are particularly significant. Then, for V^{4+} , Mn^{4+} , and Fe^{4+} , there are one, three, and four electrons on their $3d$ orbitals, respectively. We further analyzed the crystal fields of the three materials based on PDOS of different orbitals, and the energy arrangement of key states is illustrated in Fig. 3(d) and Figs. S3(b)–S3(d) [26]. For FeSi_2N_4 , three spin-up electrons occupy the orbits d_{z^2} , $d_{xy}/d_{x^2-y^2}$, and d_{xz}/d_{yz} , and a single spin-down electron occupies d_{z^2} . For MnSi_2N_4 , there are also three spin-up electrons in the orbital d_{z^2} , $d_{xy}/d_{x^2-y^2}$, and d_{xz}/d_{yz} but no spin-down electron in these states. For VSi_2N_4 , there is only one spin-up electron in the orbital d_{z^2} . As a result, the magnetic moment of the three materials is 1.0, 3.0, and 2.0 μ_B/atom , respectively. To validate our conclusion, we further

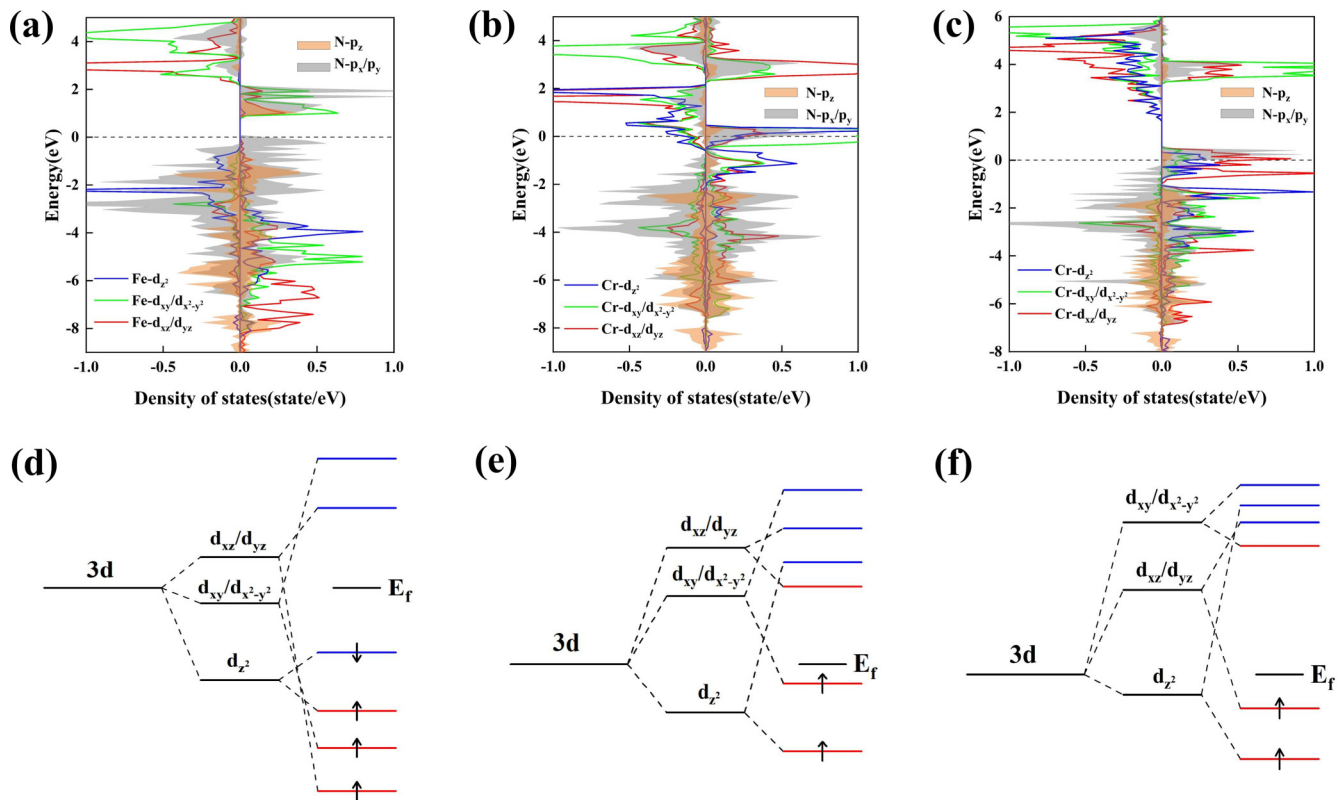


FIG. 3. PDOS and for (a) FeSi₂N₄, (b) CrSi₂N₄ when $U = 0$ and (c) CrSi₂N₄ when U is 4.40 eV, the linear response value, and (d)–(f) their corresponding crystal fields.

analyzed the magnetic moment of different materials shown in Table I and found that there are some rules in the magnetic moments' change with an increase of the number of valence electrons. For TiSi₂N₄, the magnetic moment is 0, because there is no 3d electron in Ti⁴⁺. Then, if the number of 3d electrons increases, the magnetic moment increases gradually, until the value of 3.0 μ_B /atom is achieved when $X = \text{Mn}$. From this moment, with the number of 3d electrons' increase, the magnetic moment begins to decrease, and finally to 0 when $X = \text{Ni}$. If the number of 3d electron still increases, a similar pattern can be observed. The result matches our prediction perfectly, proving our conclusion's correctness.

And, it is noticeable in Table I that the $X\text{Si}_2\text{N}_4$ series of materials have an integral magnetic moment in most cases, including $X = \text{Fe}$, Mn and V; However, there are some exceptional cases, such as in chromium. CrSi₂N₄ shows a magnetic moment of 1.6 or 1.7 μ_B /atom instead of an integral value in its phase T1, T2, and T3. It can also be explained by the PDOS and crystal field in Fig. 3. When the U value is 0, CrSi₂N₄ shows a metallic nature, and Fermi energy is crossed in both the spin-up band and spin-down channel, as shown in Figs. 3(b) and 3(e). Then, the magnetic moment tends to deviate from an integral value, and the fractional magnetic moment forms in the meantime. On the contrary, CrSi₂N₄ shows an integral magnetic moment with the value of 2.0 μ_B /atom when the U is 4.40 eV, its response value. The material exhibits the half-metallic feature, as shown in Figs. 3(c) and 3(f). There are two spin-up electrons on its 3d orbital, and they occupy d_{z^2} and d_{xz}/d_{yz} orbital separately,

making the magnetic moment of 2.0 μ_B /atom. To summarize, with the U value's increase, CrSi₂N₄ changes from metallic to half metallic, and the value of magnetic moment changes from fractional to integral in the meantime. We have also observed that MoSi₂N₄ exhibits the similar electron composition pattern with CrSi₂N₄ but shows a nonmagnetic property. We also clarified this distinction by analyzing the crystal field of MoSi₂N₄, as shown in Fig. S4 [26].

In order to further explore the magnetic anisotropic energy, we turn on the spin-orbit coupling by the second variational scheme as implemented in the VASP code and examine various magnetic anisotropies. We define the magnetic anisotropic energy as $\text{MAE} = \mathbf{E}[\text{XYZ}] - \mathbf{E}[001]$ [28], in which $[xyz] = [001]$, $[100]$, $[101]$, $[110]$, and $[111]$. These directions represent the z axis, x axis, facial diagonal of x - z plane, facial diagonal of x - y plane, and the body diagonal, respectively. The final results are shown in Fig. 4. It can be seen that all three materials have magnetic anisotropy, but their easy magnetization axes are different. For FeSi₂N₄ and VSi₂N₄, the easy magnetization axis formed is the diagonal direction of the x - y plane, which means that it has in-plane magnetic anisotropy. For MnSi₂N₄, the easy magnetization axis formed is z -axis direction, inducing the out-of-plane magnetic anisotropy.

From the analysis above, we can clearly see that the U value plays an important role in various kinds of properties in this series of materials. For example, the PDOS changes greatly and band tends to split with the U value's increase, and as the result, the magnetic moment changes from a fractional value to an integral one in the process. Therefore, it is

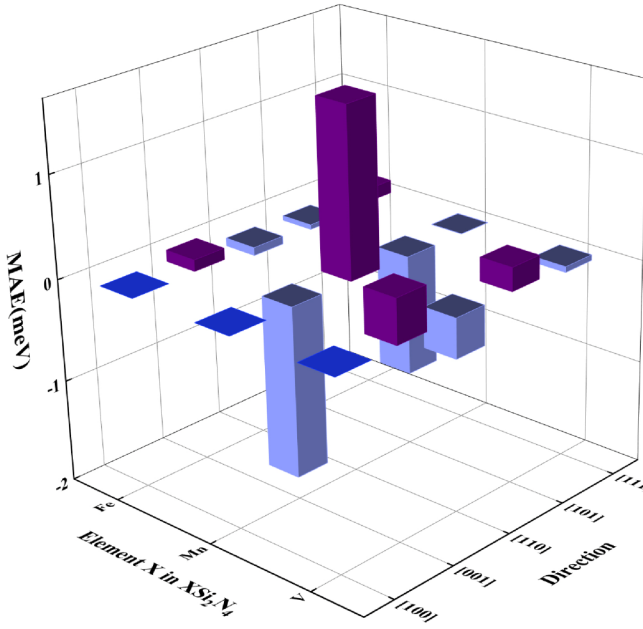


FIG. 4. Magnetic anisotropic energy (MAE) of three materials, in which MAE is defined as $\text{MAE} = E[\text{XYZ}] - E[001]$.

important to do further investigation under the materials' linear response value of U and try to analyze the internal mechanism. In Secs. IV and V, we will do further research on the Mott transition and the superexchange mechanism under the linear response value of U , then reveal its obvious significance in these two phenomena.

IV. BAND STRUCTURE AND MOTT TRANSITION

Combining with the results of the U value calculated by the linear response method, we calculated the band structures of the three materials. The calculation results of FeSi_2N_4 are shown in Fig. 5. When $U = 0$, FeSi_2N_4 presents a half-metallic property. The spin-down electron band exhibits conductor properties while the spin-up electron band exhibits semiconductor properties with a band gap of 1.53 eV. Therefore, the FeSi_2N_4 finally presents a half-metallic property. When the response value of U is 7.08 eV, the band structure changes from half-metallic to semiconductive. The band gap is an indirect one of 0.93 eV. The valence-band maximum

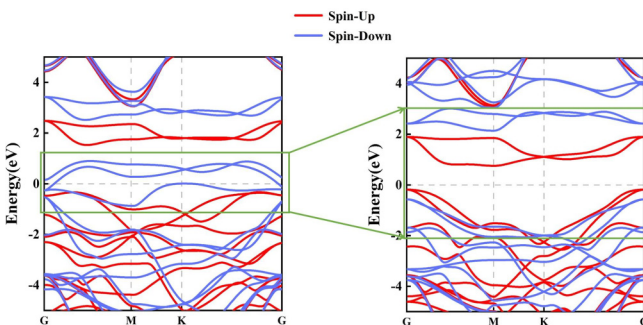


FIG. 5. Band structure of FeSi_2N_4 when $U = 0$ and the linear response value, respectively.

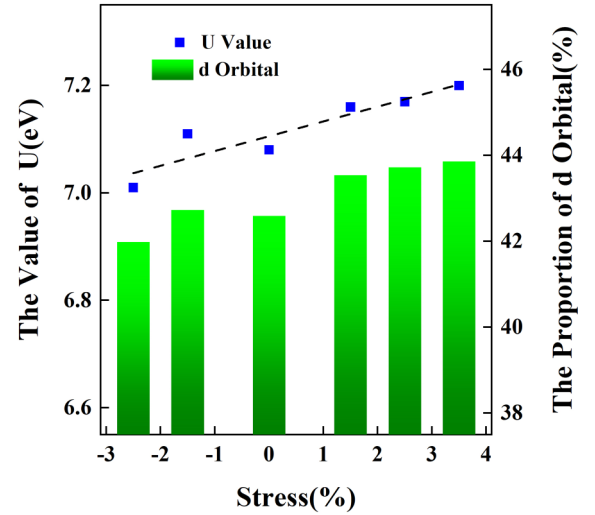


FIG. 6. Relationship of stress and U and the proportion of the d orbital in the d - p hybridization.

locates at the Γ point belonging to the spin-up channel. The bottom of the conduction band locates between Γ and M point, which is within the unoccupied spin-up band as well. The splitting of its band structure is considerable as the U value's increase. The similar phenomenon is also found in the band structures of both MnSi_2N_4 and VSi_2N_4 , which are shown in Fig. S5 [26]. For MnSi_2N_4 , its electronic structure transforms from metallic when $U = 0$ to semiconducting for $U = 5.01$ eV, with an indirect band gap of 1.26 eV. As for VSi_2N_4 , the band structure transforms from metallicity when $U = 0$ to semiconductor when $U = 5.28$ eV, with a direct band gap of 1.28 eV, which is different from the indirect band gap of the other two kinds of materials.

Owing to the visible splitting of the material's d band in the process of U value's increase, materials all have the transition from metallic or half metallic to semiconducting or insulating. The energy of the two subbands conforms to the following relationship [29]:

$$E_{k\sigma}^{(1)} \approx T_0 + (E_k - T_0)(1 - \langle n_{\sigma}^- \rangle), \quad (4)$$

$$E_{k\sigma}^{(2)} \approx U + T_0 + (E_k - T_0)\langle n_{\sigma}^- \rangle, \quad (5)$$

in which T_0 is the average energy of band electrons, U is the on-site occupancy energy, and $\langle n_{\sigma}^- \rangle$ is the occupied number of electrons with the same spin. It can be seen that the transition from metallic to semiconducting or even insulating occurs during the splitting of a single band structure into subbands, and the transition process is closely related to the magnitude of the U . As a result, various techniques, such as applying external loading to the materials, can be used to modify the strength of U , further achieving additional function based on the Mott transition mechanism.

To further clarify the Mott mechanism, we studied the effect of the stress on the U value of the materials by applying biaxial stress. In Fig. 6, we exhibit the simulated magnitudes of U under different strengths of tension or pressure. The results strongly indicate that the stress can have a significant

influence on the U value of the material, and the U value shows a significant increasing trend with the continuous increase of the stress.

According to the Hubbard model, the U value can be quantitatively expressed by the following relationship:

$$U = e^2 \int \frac{a^*(r - R_i) a^*(r' - R_i) a(r - R_i) a(r' - R_i)}{|r - r'|} dr dr' \quad (6)$$

It can be clearly seen from the above formula that the U value has a strong correlation with the degree of localization of the orbitals. The higher the degree of localization of the orbital, the greater the U value is. As a result, the strength of d - p hybridization can have great influence on the U value. To theoretically reveal the variance of U , we calculated the composition of d orbital in d - p hybridized state by using the Wannier function scheme. Herein, the equation of the Wannier function can be expressed as

$$a_n(r - l) = N^{-1/2} \sum_{k \in \text{BZ}} e^{-ikl} \phi_{nk}(r), \quad (7)$$

while the Bloch eigenstates of the Bloch function $\phi_{nk}(r)$ can be expanded as

$$|\phi_{nk}\rangle = \sum_j C_j^{nk} |\chi_j^k\rangle. \quad (8)$$

And, the Hamilton matrix can be constructed as

$$H_{ij}^k = \langle \chi_i^k | H | \chi_j^k \rangle. \quad (9)$$

Based on the formulas above, we can achieve the proportion of different orbitals from the value of C_{nk} by performing WANNIER90 program [30], and establish the connection between orbital proportions and U . Here, we use C_{nk} to show the proportion of d orbitals and do our further analysis based thereon.

On this foundation, we simultaneously calculated the Wannier function for the states of the three materials under different stresses to show the relation of the U value and localization of the orbitals. Since the hybridization mainly occurs in the spin-up electrons according to the analysis of crystal field, we chose the Gamma point and the spin-up electrons to analyze the consequence shown by the Wannier function. The result is also shown in Fig. 6 associating with the U value. It can be clearly seen that the U value of FeSi_2N_4 is very closely related to the proportion of d orbitals, and the higher d -orbital ratio can always induce the larger U . Such strongly dependent behavior further demonstrated that the U value is closely related to the degree of orbital localization. The change of the proportion of the d orbital is more significant with the change of stress and has a greater impact on the change of the U value.

Meanwhile, it can be also reasonably predicted that different control methods can be used on the material, such as stress, electric field, and so on. In this way, the U value of the material can be modified, so as to control the band structure of the material to achieve or tailor physical properties.

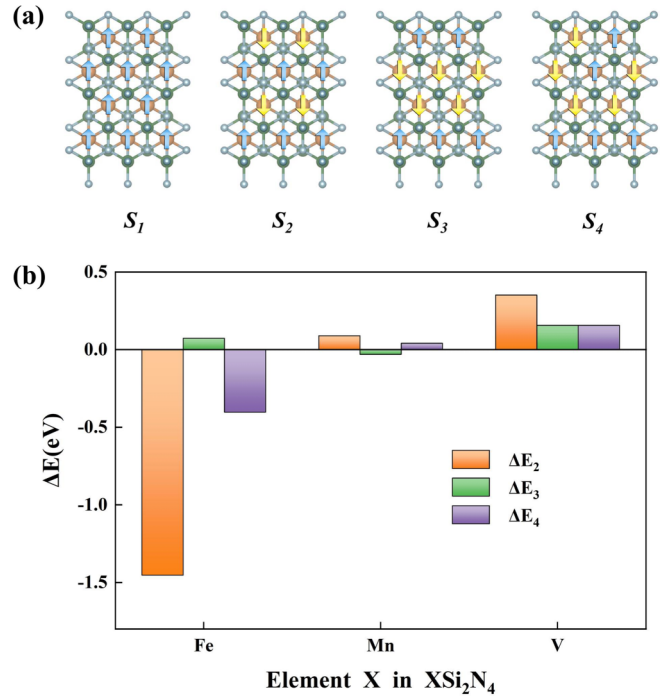


FIG. 7. (a) Schematic diagram of the state used for calculation of superexchange interaction and (b) the energy contrast of different states.

V. SUPEREXCHANGE INTERACTION OF THE MATERIAL

For metal atoms, their spins interact with each other, inducing the ferromagnetic order or antiferromagnetic order. For XSi_2N_4 system materials, the distance between the transition-metal X atoms is relatively large, suggesting that the direct exchange interaction is hard to form. Therefore, the atomic spin's interaction is realized through superexchange interaction. Firstly, we calculated the magnetic exchange coefficients of these three magnetic materials. The exchange effects are considered included near-neighboring atomic exchange, second-neighboring atomic exchange, and third-neighboring atomic exchange, which are represented by J_1 , J_2 , and J_3 , respectively. We established one ferromagnetic state and three antiferromagnetic states [31] with different spin conditions called S_1 , S_2 , S_3 , and S_4 to calculate the value of J , as shown in Fig. 7(a). The corresponding energies of these states are E_1 , E_2 , E_3 , and E_4 . Finally, we obtained our calculation formula for J as below and relevant results were obtained through calculation and put into the calculation formula of J value, which is shown in Table II. Meanwhile, we defined $\Delta E_x = E_x - E_1$, in which $x = 2, 3$, and 4 to describe the energy contrast of different states in XSi_2N_4 . It can be found that VSi_2N_4 tends

TABLE II. Table of exchange coefficients (unit: meV).

	Fe	Mn	V
J_1	13.17	1.28	-26.84
J_2	-58.59	-3.00	70.84
J_3	54.30	-1.03	-37.84

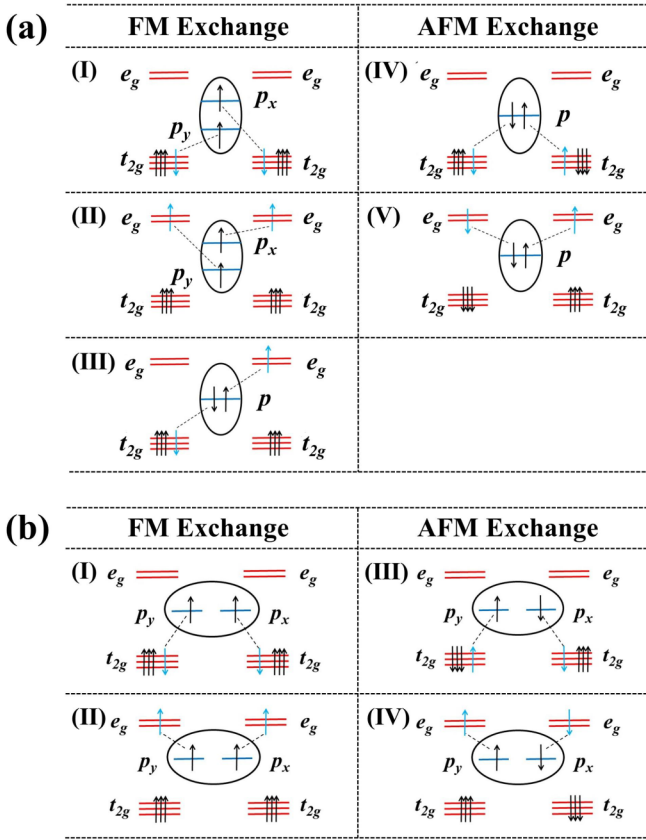


FIG. 8. Superexchange mechanism of (a) J_1 and (b) J_2 in $X\text{Si}_2\text{N}_4$.

to form the ferromagnetic order, while FeSi_2N_4 and MnSi_2N_4 tend to form the antiferromagnetic order, which is shown in Fig. 7(b).

$$16J_1 + 16J_2 = (E_2 - E_1)/2s^2, \quad (10)$$

$$8J_1 + 16J_2 + 16J_3 = (E_3 - E_1)/2s^2, \quad (11)$$

$$14J_1 + 14J_2 + 8J_3 = (E_4 - E_1)/2s^2. \quad (12)$$

Then we explored the mechanism of superexchange. The strength of the superexchange interaction is determined by the magnitude of effective J , which can be expressed as

$$J_{\text{eff}} = \frac{4t_0^4}{\Delta^2} \left(\frac{1}{\Delta} + \frac{1}{U} \right), \quad (13)$$

in which t_0 means the hopping integral of the d and p orbital, Δ means the splitting energy of the d and p orbital, and U means the on-site Coulomb interaction of d orbital. It can be clearly seen that its strength is mainly affected by two kinds of energy, namely, the charge occupation energy of the d orbital and the charge-transfer energy between the d - p orbital.

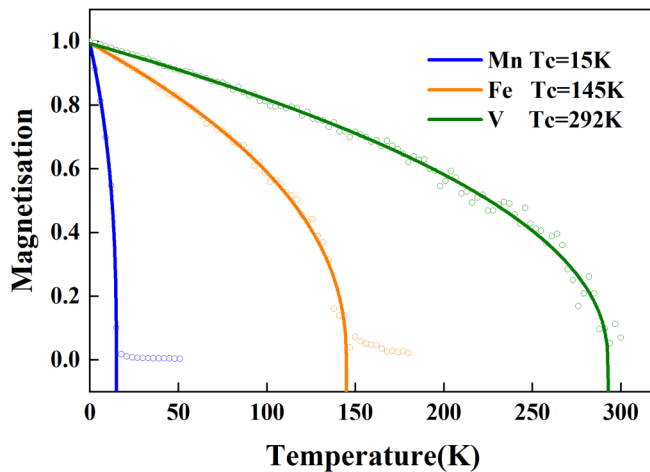
If only J_1 is considered, VSi_2N_4 tends to form an antiferromagnetic order, while FeSi_2N_4 and MnSi_2N_4 tend to form a ferromagnetic order. Combining the electron arrangement of the three materials for analysis, this result can be clarified by the mechanism below: as shown in Fig. 8(a), for $X\text{Si}_2\text{N}_4$, we raised five kinds of superexchange mechanisms [32]

according to the different d - p hybrid approach of J_1 based on the well-known GKA rule [33]. According to the rule, if the electron transfer happens between overlapping orbitals that are each half filled, the superexchange interactions are antiferromagnetic. However, they are ferromagnetic if the virtual electron transfer is from a half-filled to an empty orbital or from a filled to a half-filled orbital. The first three mechanisms make the material form a ferromagnetic order, while the latter two induce antiferromagnetic order. According to our simulation, the U value in $X\text{Si}_2\text{N}_4$ is much bigger than the splitting energy; thus, the electrons tend to fill in the e_g orbital, indicating that the mechanism (II) in ferromagnetic exchange and (V) in antiferromagnetic exchange plays the dominant role.

For mechanisms (II) and (V), the major difference concentrates on the hybridization condition of the p orbital. If the electrons locate on the same orbital, mechanism (V) dominates the superexchange interaction, forming the antiferromagnetic order. And, if they are on different orbitals, the major hybridization occurs following the mechanism (II), forming the ferromagnetic order. Therefore, we now put our eyes on PDOS of the neighboring N atom of the metal atom to obtain the electron occupy state of the p orbitals. From PDOS of three materials, we can see that in FeSi_2N_4 , the spin-up electrons play the dominated role in the hybridization, suggesting that mechanism (II) plays the dominated role in J_1 . Similarly, we can observe that in MnSi_2N_4 , the spin-up electrons induce stronger hybridization than spin-down electrons, indicating that mechanism (II) is more decisive than mechanism (V) in the forming of the magnetic order. As a result, the value J_1 of MnSi_2N_4 reveals that it tends to form a ferromagnetic ordering, but the tendency is much smaller compared to FeSi_2N_4 . For VSi_2N_4 , it is obvious that the spin-up electrons and the spin-down ones participate in the hybridization together, demonstrating that the mechanism (V) plays the critical role in hybridization, allowing VSi_2N_4 to form an antiferromagnetic ordering.

However, the magnetic order of the $X\text{Si}_2\text{N}_4$ series of materials shows a totally opposite consequence with what is revealed by J_1 . Then, we further discovered that such effect can be primarily attributed to the anomalously large J_2 for all of the three-layered materials. As shown in Fig. 8(b), compared with J_1 , there is not only the localization effect of d - p hybridization but also the delocalization effect of p - p hybridization. The delocalization of p - p bonding is substantially stronger than the localization of d - p bonding in $X\text{Si}_2\text{N}_4$ due to the strong nonmetallicity of N and the fact that the p - p link only exists between the p_x/p_y two orbitals, implying that the effect is more significant, as is shown in Fig. 8(b). Therefore, the final result is that the value of J_2 is much greater than J_1 . Thus, J_2 plays the predominant role in the forming process of the magnetic order. We further analyze the effect of J_3 on the magnetic orders, which is summarized in Part S7 in the Supplemental Material [26].

Furthermore, we performed Monte Carlo simulation via the VAMPIRE software [34] package to derive the Curie temperatures for $X\text{Si}_2\text{N}_4$. As shown in Fig. 9 below, the Curie temperature can reach up to 145 K for FeSi_2N_4 , and 292 K for VSi_2N_4 , respectively.

FIG. 9. Curie temperature of $X\text{Si}_2\text{N}_4$.

VI. CONCLUSION

In this work, we focused on the $X\text{Si}_2\text{N}_4$ series of materials, replaced Mo element with different transition-metal elements $X = \text{Ti}, \text{V}, \text{Cr}, \text{Mn}, \text{Fe}, \text{Co}, \text{Ni},$ and Cu , and did further research when $X = \text{Fe}, \text{Mn},$ and V . We explored their respective magnetic properties, such as the magnetic moment, magnetic anisotropy, the exchange coefficient J , and the Curie temperature, etc. Furthermore, we discovered that the band-structure formation mechanism inside the material is the Mott mechanism. We further explored the formation process of the

Mott mechanism in combination with the Wannier functions under the biaxial strain loadings. Finally, to explain the result of the internal magnetic order's formation of the materials, we analyzed the superexchange mechanism, calculated the value of the superexchange coefficient J and explained the consequence, then gained a deeper understanding in the formation process of the internal magnetic order. We hope to further discover the mechanism of the magnetism in this series of materials in the future, guiding the development of the two-dimensional magnetic materials.

ACKNOWLEDGMENTS

Y.W. acknowledges support by the Undergraduate Innovation and Entrepreneurship Training Program of Beihang University (Grant No. X202110006006). D.L. acknowledges support by the European Regional Development Fund in the IT4Innovations national supercomputing center—Path to Exascale project (Grant No. CZ.02.1.01/0.0/0.0/16_013/0001791) within the Operational Programme Research, Development and Education and the project e-INFRA CZ (Grant ID No. 90140) by the Ministry of Education, Youth, and Sport of the Czech Republic. Q.Z. acknowledges support by the Beijing Natural Science Foundation (Grant No. 2192029), the National Key Research and Development Program of China (Grant No. 2017YFB0702100) and the National Natural Science Foundation of China (Grant No. 11404017).

- [1] K. S. Novoselov, A. K. Geim, S. V. Morozov, D. Jiang, Y. Zhang, S. V. Dubonos, I. V. Grigorieva, and A. A. Firsov, *Science* **306**, 666 (2004).
- [2] K. S. Novoselov, D. Jiang, F. Schedin, T. J. Booth, V. V. Khotkevich, S. V. Morozov, and A. K. Geim, *Proc. Natl. Acad. Sci. USA* **102**, 10451 (2005).
- [3] J. Park, J. Joo, S. G. Kwon, Y. Jang, and T. Hyeon, *Angew. Chem. Int. Ed.* **46**, 4630 (2007).
- [4] B. Huang, G. Clark, E. Navarro-Moratalla, D. R. Klein, R. Cheng, K. L. Seyler, D. Zhong, E. Schmidgall, M. A. McGuire, D. H. Cobden, W. Yao, D. Xiao, P. Jarillo-Herrero, and X. D. Xu, *Nature (London)* **546**, 270 (2017).
- [5] G. R. Bhimanapati, *ACS Nano* **9**, 11509 (2015).
- [6] Y. L. Hong, Z. B. Liu, L. Wang, T. Y. Zhou, W. Ma, C. Xu, S. Feng, L. Chen, M. L. Chen, D. M. Sun, X. Q. Chen, H. M. Cheng, and W. C. Ren, *Science* **369**, 670 (2020).
- [7] Q. Cui, Y. Zhu, J. Liang, P. Cui, and H. Yang, *Phys. Rev. B* **103**, 085421 (2021).
- [8] S. D. Guo, W. Q. Mu, Y. T. Zhu, and X. Q. Chen, *Phys. Chem. Chem. Phys.* **22**, 28359 (2020).
- [9] A. Bafekry, M. Faraji, M. M. Fadlallah, A. B. Khatibani, A. A. Ziabari, M. Ghergherehchi, S. Nedaei, S. F. Shayesteh, and D. Gogova, *Appl. Surf. Sci.* **559**, 149862 (2021).
- [10] M. R. K. Akanda and R. K. Lake, *Appl. Phys. Lett.* **119**, 052402 (2021).
- [11] A. Ray, S. Tyagi, N. Singh, and U. Schwingenschlogl, *ACS Omega* **6**, 30371 (2021).
- [12] I. Bloch, J. Dalibard, and W. Zwerger, *Rev. Mod. Phys.* **80**, 885 (2008).
- [13] M. J. Han and J. Yu, *J. Korean Phys. Soc.* **48**, 1496 (2006).
- [14] S. Telemeter, W. Weber, J. Schulenburg, and J. Richter, *Phys. Rev. B* **52**, 313 (1995).
- [15] G. Kresse and J. Furthmüller, *Phys. Rev. B* **54**, 11169 (1996).
- [16] G. Kresse and J. Furthmüller, *Comput. Mater. Sci.* **6**, 15 (1996).
- [17] J. P. Perdew, K. Burke, and M. Ernzerhof, *Phys. Rev. Lett.* **77**, 3865 (1996).
- [18] P. E. Blochl, *Phys. Rev. B* **50**, 17953 (1994).
- [19] G. Kresse and D. Joubert, *Phys. Rev. B* **59**, 1758 (1999).
- [20] H. J. Monkhorst and J. D. Pack, *Phys. Rev. B* **13**, 5188 (1976).
- [21] V. I. Anisimov, F. Aryasetiawan, and A. I. Lichtenstein, *J. Phys.: Condens. Matter* **9**, 767 (1997).
- [22] M. Cococcioni and S. de Gironcoli, *Phys. Rev. B* **71**, 035105 (2005).
- [23] H. J. Kulik, M. Cococcioni, D. A. Scherlis, and N. Marzari, *Phys. Rev. Lett.* **97**, 103001 (2006).
- [24] A. Togo, and I. Tanaka, *Scr. Mater.* **108**, 1 (2015).
- [25] V. Wang, N. Xu, J. C. Liu, G. Tang, and W. T. Geng, *Comput. Phys. Commun.* **267**, 108033 (2021).

- [26] See Supplemental Material at <http://link.aps.org/supplemental/10.1103/PhysRevB.106.104421> for Figs. S1–S6, Table S1, and supplemental notes about additional detailed calculation scheme, phonon spectra, electronic structures, and the superexchange mechanism of J3.
- [27] L. Wang, Y. P. Shi, M. F. Liu, A. Zhang, Y. L. Hong, R. H. Li, Q. Gao, M. X. Chen, W. C. Ren, H. M. Cheng, Y. Y. Li, and X. Q. Chen, *Nat. Commun.* **12**, 2361 (2021).
- [28] X. Liu, D. Legut, R. Zhang, T. Wang, Y. Fan, and Q. Zhang, *Phys. Rev. B* **100**, 054438 (2019).
- [29] *Solid State Theory*, edited by Z. Li (Higher Education Press, Beijing, 2002).
- [30] A. A. Mostofi, J. R. Yates, G. Pizzi, Y.-S. Lee, I. Souza, D. Vanderbilt, and N. Marzari, *Comput. Phys. Commun.* **185**, 2309 (2014).
- [31] C. Wang, X. Zhou, Y. Pan, J. Qiao, X. Kong, C. C. Kaun, and W. Ji, *Phys. Rev. B* **97**, 245409 (2018).
- [32] J. Xiao, D. Legut, W. Luo, H. Guo, X. Liu, R. Zhang, and Q. Zhang, *Phys. Rev. B* **101**, 014431 (2020).
- [33] J. B. Goodenough, *Scholarpedia*, 3(10):7382, revision No. 122456 (2008).
- [34] R. F. L. Evans, W. J. Fan, P. Chureemart, T. A. Ostler, M. O. A. Ellis, and R. W. Chantrell, *J. Phys.: Condens. Matter* **26**, 103202 (2014).